3556–3572 *Nucleic Acids Research, 2023, Vol. 51, No. 8* *Published online 20 March 2023*
https://doi.org/10.1093/nar/gkad179

Cavity hairpin ThT-light nucleic acid switches: the construction of label- and enzyme-free sensing and imaging platforms

Xinyue Lan[1,2,†], Longjiao Zhu[1,†], Yangzi Zhang[1,2], Keren Chen[1,2], Jia Wang[1], Zaihui Du[1,2], Shuting Li[1,2], Xu Chen[1,2] and Wentao Xu[1,*]

[1]Food Laboratory of Zhongyuan, Key Laboratory of Precision Nutrition and Food Quality, Department of Nutrition and Health, China Agricultural University, No. 17, Qinghua East Road, Beijing 100193, China and [2]Key Laboratory of Safety Assessment of Genetically Modified Organism (Food Safety), College of Food Science and Nutritional Engineering, China Agricultural University, No. 17, Qinghua East Road, Beijing 100083, China

Received October 23, 2022; Revised February 01, 2023; Editorial Decision February 23, 2023; Accepted March 16, 2023

ABSTRACT

Thioflavin T (ThT) is a classical fluorescent dye gaining prominence in current research regarding nucleic acid conformations (NACs). However, most NACs with the ability to excite ThT fluorescent are unique or form in demanding conditions, limiting the extensiveness and depth of ThT application in sensing and imaging. Therefore, this study proposed CGG-AAA mismatched cavity hairpin ThT-light nucleic acid switches (CHTLNAS) with excellent fluorescence excitation over 500-fold higher than spontaneous, 17∼20-fold higher than ssDNA and 2.5∼5-fold higher than complementary duplex. Based on the excellent fluorescence excitation, convenient conformation formation, good sequence programmability, and flexible allosteric ability (known as the *Worm-crack pod* mechanism mediated by the target), it achieved the label- and enzyme-free detection of tetracycline (TET) and berberine (BB) at the pM level within 10 min. Moreover, it was found enable to realize the sensitive tracking of intracellular carriers at the nM level of ThT entry concentration, and prolongated its cell nuclear-entry time of ThT over 8 h, overcoming the non-specific high background signal interference of ThT in the nuclear region, and expanding the diversified application of ThT in cell biology research. Therefore, CHTLNAS is a more universal, practical tool than G-quadruplex or other kinds of NACs for ThT development and utilization in sensing and imaging platforms.

GRAPHICAL ABSTRACT

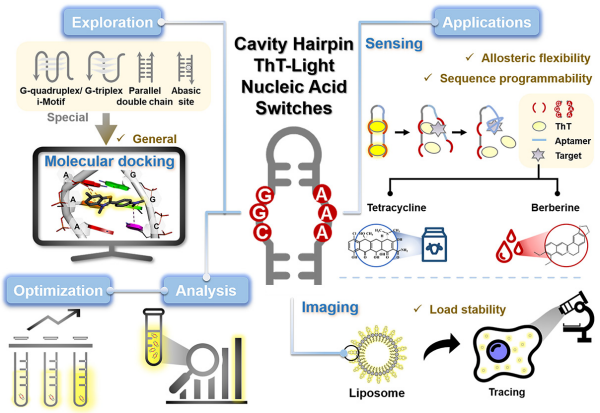

INTRODUCTION

Thioflavin T (ThT) is a common fluorescent dye whose use can be traced back to the middle of the last century and was first reported for the quantitative analysis of amyloid in thyroid and kidney tissue sections (1,2). By the end of the 20th century, scientists expanded ThT application from the histological analysis (3,4) to structure and disease studies (5–7) playing a substantial role in biomedical research. Besides, it was found to be lighted by single stranded DNA containing purine bases but not pyrimidine as early as 1973 (8). In the past decade, ThT fluorescent were systematically reported to be excited by various kinds of nucleic acid sequences with different conformations, accompanying by the advantages of photophysical stability, membrane permeability and low toxicity (9), it can not only point the conformational changes of nucleic acids for exploring its biological function, but also replace the traditional fluorescent labels for imaging intracellular distribution of nucleic acid

*To whom correspondence should be addressed. Tel: +86 10 6273 8793; Email: xuwentao@cau.edu.cn
†The authors wish it to be known that, in their opinion, the first two authors should be regarded as Joint First Authors.

conformations (NACs), even monitor the expression and metabolism process of genes with specific nucleic acid structures (9,10). However, the emergence of ThT in key areas of current nucleic acid research has emphasized some deficiencies requiring attention (11,12). The concentration (μM) or developed nanocarriers (10) were increased to overcome the challenges presented by a high background signal and limited fluorescence excitation in cells and achieve a similar effect to commonly used nucleic acid dyes. Thus, exploring novel NACs for ThT lighting and loading is necessary to promote its intracellular imaging development.

G-quadruplexes (G4) represent a typical conformation for ThT lighting. Jyotirmayee et al. achieved a nearly 2100-fold enhancement of ThT fluorescence when binding it to human telomeric G4 in the presence of K^+ (13). Furthermore, it was proposed that the reason for ThT fluorescence excitation was that G4 provided ThT with suitable insertion room via G-quartet formation, allowing its benzothiazole (BZT) and dimethylbenzyl (DMAB) rings to be on the same plane, restricting the free rotation of C–C (14) to limit the transformation ThT state from locally excited to twisted intramolecular charge transfer (15). Although G4 leads ThT as a mainstream fluorescent tool for NAC indication nowadays (16–18), the extra supply of K^+ or Na^+ solution environment is required for G4 stably forming, as well as the large quantities of G4 in genome cannot be specifically image and distinguished by ThT. These limitations were scientifically recognized, prompting the exploration of other types of NACs.

Recently, non-G4 structures, G-triplexes (19), i-motifs (20), and duplexes (21–24) were reported for ThT lighting. Some unique conformations like base aberrations, bulges, mismatches, and abasic sites are more likely to appear in duplexes (25,26), while parallel duplexes containing GA accompanied by over 100-fold ThT fluorescence enhancements perform even better than some G4 sequences (21). Compared with G4, duplex conformations are more easily formed and assembled to integrate and amplify the ThT signal, showing extensive promise in the sensing and mutagenic diagnostic fields. However, further research is required regarding the ThT fluorescent excitation mechanism of duplexes to provide more detailed guidance on potential conformations and eliminate the complicated process involved in the ThT lighting sequence screening of a large number of samples. Moreover, most duplexes available for ThT lighting are unconventional, requiring the introduction or creation of extra specific nucleic acid sequences, such as abasic sites and parallel duplexes, to support the conformational formation.

Therefore, considering the ThT fluorescence intensity are not only determined by the binding affinity, but also the factor of NAC's topological structure (13), as well as inspired by the mutation and bubbling (27) that might occur during DNA processing, and the widely accepted ThT 'light-switch' mechanism (15), we explored the A-C/A-G/A-G (CGG-AAA) cavity hairpin ThT-light nucleic acid switches (CHTLNAS) based on the combination of computer prediction and actual sequence verification. which has a stronger sequence programmability of the target section and a more conventional duplex conformation less subject to the restrictions imposed by formational conditions, serving as a universal tool for effective fluorescent excitation and extending the application in the sensing and cellular imaging at the nucleic acid level on ThT.

MATERIALS AND METHODS

Materials

Tetracycline (TET), berberine (BB), kanamycin, ampicillin, doxycycline, oxytetracycline, gentamicin, chloramphenicol, lincomycin, baicalin, capsicine, betaine, cannabidiol, glycine, gluutamine, tyrosine, ascorbic, Dulbecco's PBS (DPBS), thioflavin T (ThT), acetonitrile, trichloromethane, 1,2-dimyristoyl-sn-glycero-3-phosphocholine (DMPC), and cholesterol were purchased from Sigma-Aldrich (St. Louis, MO). All chemical reagents were analytical grade and were used as received without further purification. The ultrapure water (UP) used throughout all experiments was purified by a Milli-Q system (Millipore, Bedford, MA, USA). The raw liquid milk was purchased from the local pasture. 4% (w/v) paraformaldehyde, Hoechst 33342 and DiD dye were purchased from Beyotime Biotechnology (Shanghai, China).

High-performance liquid chromatography purified oligonucleotides (ODNs) were purchased from Shanghai Sangon Biological Engineering Technology & Services (Shanghai, China), and used without additional purification (See Supplementary Table S1 for details of DNA sequences used). Each sequence was diluted in UP into 100 μmol l^{-1}. For better formation of secondary conformation, sequences were heated to 95 °C for 5 min and colded to room temperature overnight, and was stored at −20 °C before use.

Prediction of nucleic acid conformation and molecular docking

The docking experiments were performed using HDOCK server (http://hdock.phys.hust.edu.cn/). The input receptor molecules were the 3D structures of nucleic acids sequences which transformed the RNA structure who acquired from the RNA Composer server (http://rnacomposer.ibch.poznan.pl/) after the 2D structures were predicted by MC-fold server (https://major.iric.ca/MC-Pipeline/) into DNA via Discovery studio 2021 software. The input ligand molecule acquired from PubChem (https://pubchem.ncbi.nlm.nih.gov/), and were minimized energy by Chemoffice software. The docking results were analyzed by Discovery studio 2021 software, docking conformations were evaluated according to the CScore.

The secondary conformation of nucleic acid sequences were drew by NUPACK server (http://www.nupack.org/partition/new).

Fluorescence measurements

Fluorescence spectra were recorded on a Cary Eclipse fluorescence spectrophotometer (Agilent Technologies, Inc., CA, USA). Before optimizing the detection system, sequence was introduced into 10 mmol l^{-1} Tris-HCI buffer (pH 7.4) to meet the final concentration with 1 μmol l^{-1},

then ThT or SYBR Green I (10 000×) or BB was introduced to above solution to meet the final concentration with 1 μmol l^{-1} and let the total volume of the solution to be analyzed to 100 μl, stirred thoroughly at room temperature for 5 min. The fluorescence emission spectra of ThT sensing system were monitored as 470–600 nm with an excitation wavelength of 445 nm; the fluorescence emission spectra of SYBR Green I sensing system were monitored as 510–620 nm with an excitation wavelength of 497 nm; The fluorescence emission spectra of BB sensing system were monitored as 480–600 nm with an excitation wavelength of 365 nm.

Fluorescence kinetics measurement

The incubation time optimization in sensor establishment. Sequence introduced into 10 mmol l^{-1} Tris-HCI buffer (pH 7.4) to meet the final concentration with 1 μmol l^{-1}, ThT was introduced to above solution to meet the final concentration with 2 μmol l^{-1}, stirred thoroughly at room temperature for 5 min. Upon the kinetics measurement was started, target solution containing TET/BB, or UP was introduced to the system immediatelylet the total volume of the solution to be analyzed to 100 μl. The fluorescence emission wavelength was 490 nm, the excitation wavelength was 445 nm, the read interval was 0.02 s.

The ThT-competitive-ability evaluation between hairpins with or without cavity. The 1 μmol l^{-1} ThT was first introduced into 10 mmol l^{-1} Tris-HCI buffer (pH 7.4), stirred thoroughly at room temperature for 5 min to let the fluorescence stable, and then start the kinetics measurement. The complementary hairpin and cavity hairpin with equal concentration was alternately added 0.1 μmol l^{-1} into the system every 1 min. End the monitoring procedure until the ThT fluorescence no longer increases with either sequence addition. The fluorescence emission wavelength was 490 nm, the excitation wavelength was 445 nm, the read interval was 0.02 s.

UV-visible absorption spectroscopy

A UV2800 UV-vis spectrometer (UNICO, USA) was utilized to collect the absorption spectra of a mixture of 2.5 μmol l^{-1} ThT and 0/1/2/3/4/5 μmol l^{-1} sequcence in 10 mmol l^{-1} Tris-HCI buffer (pH 7.4). Three scans from 380 to 500 nm were accumulated and averaged. The background absorption of the buffer solution was subtracted from the data.

Fluorescence sensing of targets

Sequence was introduced into 10 mmol l^{-1} Tris-HCI buffer (pH 7.4) to meet the final concentration with 1 μmol l^{-1}, the targets with final concentrations range of 500 pmol l^{-1}–500 μmol l^{-1} was introducted in and vortex-mixed with sequcens at room temperature for 8 min. Then, ThT was introduced to above solution to meet the final concentration with 2 μmol l^{-1} and let the total volume of the solution to be analyzed to 100 μl, stirred thoroughly at room temperature for 5 min. The LOD calculated by the formula $LOD = 3\sigma/K$, where σ is the standard deviation of the blank sample (without target) and K is the slope of the standard curve, according to the rule of 3 times the standard deviation of the blank signal.

Affinity analysis

The affinity (K_d) was determined by monitoring the increase of the fluorescence intensity of ThT after binding with CHTLANS. Different concentrations (from zero to saturation) of CHTLANS were dissolved in the 10 mmol l^{-1} Tris-HCI buffer (pH 7.4), and then incubated ThT to meet the final concentration with 4 μmol l^{-1}, and let the total volume of the solution to be analyzed to 100 μl, stirred thoroughly at room temperature for 5 min. Under the excitation wavelength of 445 nm, the fluorescence intensity at the emission wavelength of 490 nm was choose to calculated the nonlinear fitting curve (titration curve), and K_d was obtained by nonlinear fitting using the GraphPad prism 8.

Melting temperature measuring

Cary Eclipse fluorescence spectrophotometer, equipped with a thermoelectrically controlled cell holder, was used to perform melting experiments. The annealed sequence was introduced into 10 mmol l^{-1} Tris-HCI buffer (pH 7.4). A temperature range of 25–95 °C was used to monitor the changes of SGI at a heating/cooling rate of 0.3 °C/min. The temperature-dependence fluorescence intensity of sequence was analyzed using GraphPad prism 8.

Specific detection

The selective detection for tetracycline. 1.25 μmol l^{-1} TET and 12.5 μmol l^{-1} antibiotics likely proned to residues in milk namely kanamycin, ampicillin, doxycycline, oxytetracycline, gentamicin, chloramphenicol, lincomycin were selectived to investigate the anti-interference of the TET detection.

The selective detection for berberine. 1.25 μmol l^{-1} BB and 12.5 μmol l^{-1} kinds of plant extract including baicalin, capsaicin, betaine, cannabidiol and kinds of common natural biochemical molecules including glycine, threonine, tyrosine, and ascorbic acid were selectived to investigate the anti-interference of the BB detection.

Actual sample detection

The tetracycline detection in milk samples. The pretreatment procedure for the real raw milk samples was carried out according to the published work (28), with the typical operation described as follows. Firstly, 2 mL raw milk spiked into certain amount of TET was placed into a 10 ml centrifuge tube, and diluted with water to 5 ml, then, 2 ml of 10% trichloroacetic acid and 2 ml chloroform were added and mixed under vortex for 1 min to deposit protein and dissolve fat and other organic substances in the sample matrix. For removing the protein, fat and other organic substances, the mixture was then ultrasonically treated at 20 °C for 10 min and centrifuged at 12 000 rpm for 10 min to separate

the deposit. Secondly, the supernatant was transferred into another centrifuge tube and centrifuged at 12000 rpm for 10 min to remove the deposit once again and get the final supernatant. Finally, the obtained supernatant was diluted 5 times for detection according to the procedure in Section 2.6 A, then pretreated and analyzed in accordance with the above procedure.

The berberine detection in plasma samples. The pretreatment procedure for the plasma samples was carried out according to the published work (29), with the typical operation described as follows. Firstly, 3 mL of chloroform was added to 500 μl human plasma which spiked into certain amount of BB and mixed under vortex for 2 min and centrifuged at 4000 rpm for 10 minutes. Then, the organic phase was transferred to a centrifuge tube and evaporated to dryness at 40 °C under a gentle stream of nitrogen. The residue was redissolved of mobile phase consisting of acetonitrile and water (1:2, v/v), vortexed for 30 s, sonicated for 10 min, and centrifuged at 4000 rpm for 5 min. The supernatant was used as the final sample solution. Finally, the obtained supernatant was diluted 5 times for detection according to the procedure in Section 2.6 A, then pretreated and analyzed in accordance with the above procedure.

Preparation and characterization of HC-Lip+ThT/H-Lip+ThT

The DMPC and cholesterol with the concentration ratios of 10:6 were mixed in chloroform at 37 °C until the all organic phases were evaporated under the reduced-pressure-rotary evaporation and nitrogen-purged. And then the product were respectively diluted with DEPC water at 37 °C, with a vortex time of 30 min. The mixture was then at ultrasonic condition in 37 °C for 10 min, centrifuge at 5000 g for 5 min, and the precipitate was discarded to obtain 10 mmol l^{-1} liposome solution (DMPC molar amount), which stored at 4 °C.

3H3Md-TET-3′chol or 3H-TET-3′chol was conjugated to the surface of liposomes at a mole ratio of nucleic acid to phospholipid is 500:1 in 37 °C for 6 h, centrifuge at 5000 g for 5 min, and obtain 5 mmol l^{-1} HC-Lip/H-Lip (DMPC molar amount). Then ThT was added to above system for 30 min at 37 °C in darkness, which final concentration is twice the nucleic acid sequence, obtain 1 mmol l^{-1} HC-Lip+ThT/H-Lip+ThT (DMPC molar amount), and the synthesized was stored at 4 °C.

The Size and PDI of the samples were detected using a Zetasizer Nano ZS90 (Malvern, UK). 1 ml 100 μM sample (DMPC molar amount) was placed in a sample pool to measure the particle size distribution of the system.

Cell culture

3T3-L1 cells were purchased from the Cell Bank, Chinese Academy of Sciences. Both cells were cultured in DMEM medium supplemented with 10% (v/v) FBS and 1% (v/v) penicillin-streptomycin at 37 °C in a humid atmosphere with 5% CO_2. Cell density was determined using a Countess™ II Automated Cell Counter (Thermo Fisher Scientific, UK).

Confocal microscopy

3T3-L1 cells with a density of 2×10^5 cells were cultured in μ-Slide 8 Well (ibidi GmbH, Germany). After 24 h proliferation, change the medium, then treat cell with 100 μl HC-Lip+ThT/H-Lip+ThT (dyed with DiD for 15min) containing serial, which the final concentration of ThT is 200 nmol l^{-1}. Next, follow by another 4–16 h incubation. The culture medium was removed carefully, and cells were washed with DPBS and fixed with 4% paraformaldehyde for 15 min at room temperature. After being treated with the blocking solution (DPBS containing 0.1% Triton X-100), followed by washing 3–5 times with DPBS. Finally, Hoechst 33342 was added and then incubated for 30 min at room temperature to label the cell nuclei. Samples were observed by CLSM (LSM900, Carl Zeiss, Germany).

Statistical analysis

A paired t-test and multiple comparison method were used to test for significant differences in the experimental data using SPSS 17.0 (SPSS Inc., USA). All measurements were performed in triplicate at least, and results were expressed as an average with the standard deviation.

RESULTS

The exploration of the possible mismatched cavity hairpin for ThT binding and lighting

This study designed DNA hairpins consisting of A-T base pairs (Supplementary Table S1). A-A, A-G and A-C mismatched base pairs were constructed to form a single cavity and analyzed via molecular docking. As shown in Figure 1A, the expected ThT binding (light green box area) to the A-A site did not occur, suggesting that this mismatch was not preferred for ThT binding over the other sites in the sequence. Although ThT docked better with A-G and A-C mismatched pockets, the size of them are not completely suitable for ThT inserting. It can be seen from the Figure 1 and Supplementary Figure S1 that the base pairs on the adjacent positions of cavity also provide the force for ThT binding, suggesting that the size of the single base pairs mismatch cavity is not large enough to limit the intramolecular ThT torsions, and which still need the further exploring. Therefore, considering the molecular size of ThT and the conformational stability of the formed cavity (26,30), this study proposed that the cavity sizes available for ThT intercalation and efficient lighting may consist of 2–3 mismatched base pairs.

Since the A-C and A-G single cavities presented better docking results, they were consequently selected for constructing the double mismatched base cavities. In terms of docking score and receptor-ligand interactions, the A-C/A-G cavities displayed a higher possibility of binding with ThT than a single cavity. The two planar rings of ThT were nearly parallel to the base planar at the binding pocket (Figure 1B and Supplementary Figure S1), implying that this cavity was more suitable for ThT insertion.

Therefore, a triple pairs of mismatched bases cavity was subsequently constructed using A-C/A-G. Compared with the single and double cavity groups, the forces of

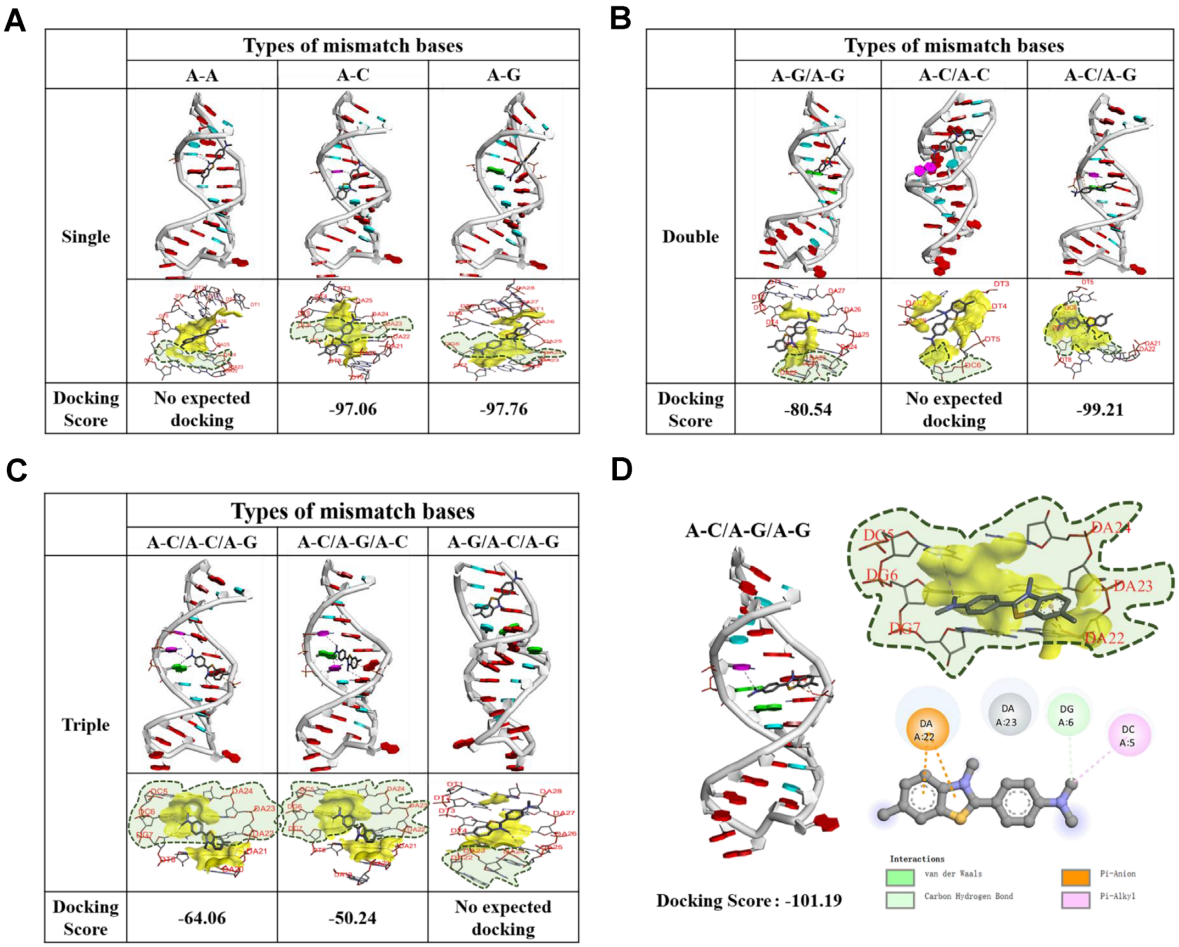

Figure 1. The overall three-dimensional structure of the molecular docking between the ThT and hairpin with single (**A**), double (**B**), or triple (**C**) (CGG-AAA cavity (**D**)) pairs of mismatched bases. The light green area represents the expected docking region, while the yellow area represents the actual docking pocket.

the receptor-ligand interactions in each triple cavity group tended to be similar, except for the A-G/A-C/A-G group (Figures 1C and D, Supplementary Figure S1), which means that with the increase of the base pairs number constituting the mismatched cavity, the homogeneity of its docking results is increase, suggesting the mismatched cavity serves as the pockets available for molecular docking tend to be single and stable. So that the triple pairs of mismatched bases cavity may have better attraction for the binding of small molecules, and a greater possibility that it will actually happen, although the results of molecular simulation docking exist certain randomness cannot avoid (31). Further, it implies that the three mismatched base pairs may form the optimal cavity size for ThT, while the A-C/A-G/A-G (CGG-AAA) mismatch provides the best docking results (Figure 1D). The A base contributes to cavity formation by mainly interacting with the ThT BZT ring via π-π bonds and Van der Waals forces, while the C and G bases primarily interact with the aminomethyl group on the ThT dimethylamino ring in the form of hydrogen and π-π bonds, which is consistent with the docking results of other groups. The CGG-AAA mismatch cavity showed the best docking effect, which could be because the A-C base mismatch consists of purine-pyrimidine, providing a looser pocket for ThT insertion due to the size effect and weaker non-Watson-Crick base pairs than A-G or A-A, allowing quicker ThT entry (26,32,33). For the G-A mismatch, the interaction between the G base and the ThT aminomethyl group appeared in almost every docking result, suggesting that the presence of the G base positively affected ThT binding with the cavity. The G-A mainly played a 'supporting' role similar to the 'platform.' ThT entry into the vicinity of the C-A cavity improved communication between the G base and the opposite A base via interaction with the ThT benzothiazolium and dimethylamino rings to facilitate appropriate positioning. Therefore, ThT could bind better with the cavity, restricting the free rotation of its two rings.

Consequently, this study proposed that the A-C mismatch mainly provided an initial readily insertable site for ThT, while the A-G mismatch presented a platform that supported stable ThT insertion via the interaction between the G base and the opposite A bases, further confirming why A bases displayed good ThT fluorescence emission in the non-G4 sequence. Therefore, we have reason to believe that the duplex containing CGG-AAA mismatched cavity could possible lighting ThT.

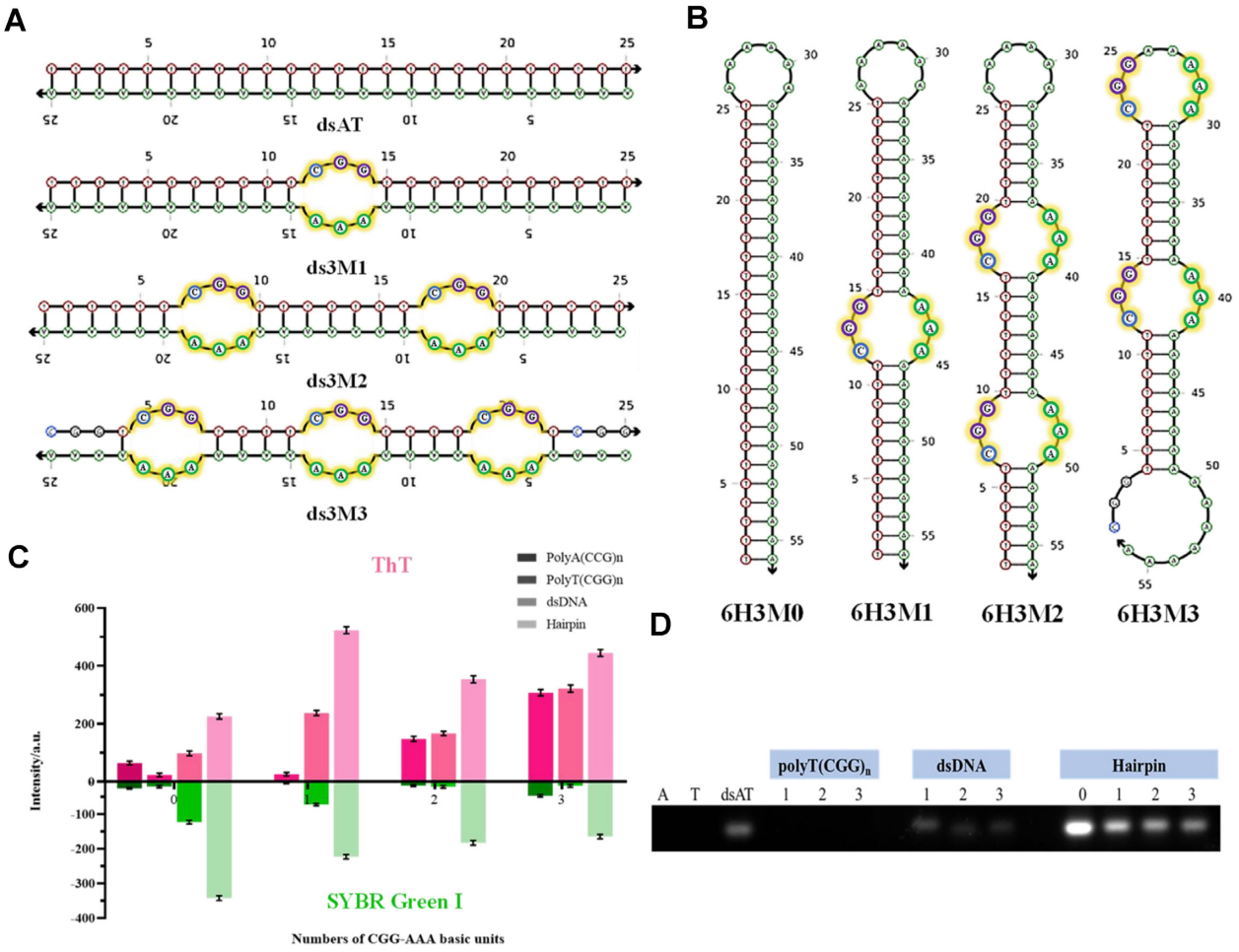

Figure 2. The assessment of CGG-AAA cavity structure lighting ThT at nucleic acid sequence with non-functional nucleic sequences. The predicted secondary structure of the (**A**) double chain and (**B**) hairpin construction of non-functional nucleic acid sequences with CGG-AAA cavities. The (**C**) ThT/SGI excitation ability and (**D**) electrophoretic results of the non-functional nucleic acid sequences with CGG-AAA cavities.

The CGG-AAA cavity hairpin shows significant potential as ThT-light switches

In view of the molecular docking results, we synthesized the A-T complementary paired double strands, hairpins, and the corresponding conformation contains 0 to 3 CGG-AAA cavities (Supplementary Table S1) (Figure 2A, B), so as to verify its actual excitation effect on ThT. In Figure 2C, the group without cavity shows the double-strand enables to light up ThT more effectively than the single chain without senior conformation, as well as the fluorescent emission of poly A is higher than poly T, which are consistent with the conclusions of previous studies (21,26,34), reflecting the positive effect of A base on ThT lighting. Further, it can be seen that in the group with same numbers of CGG-AAA cavities, the highest fluorescence of ThT emission all achieved by the hairpin conformation. To finding the reason, we explored the formation of each duplex via agarose electrophoresis and fluorescence of SYBR Green I (SG I) (Figure 2C, D), which is a dye with green excitation binds to the minor groove of dsDNA, the autofluorescence of it is very weak until binding to double-stranded DNA (35,36). The results about the hairpins obviously show a higher fluorescence of SGI and a brighter electrophoresis band than other conformations, suggest that fluorescence enhancement may be mainly attributed to the introduction of hairpin loops, which facilitate two arms of hairpin to pair complementary with a higher probability than double strand, so that the duplex and cavity can formed better for ThT lighting.

When one CGG-AAA cavity was introduced into duplex, the complementarity of hairpin is not significantly affected, and a nearly 2.5-fold ThT fluorescence excitation than the complementary hairpin was achieved, imply the positive effect of CGG-AAA mismatched for ThT lighting. As the further increasing numbers of mismatched CGG-AAA units, the duplex complementarity was greatly reduced. Especially for the dsDNA group, it can be seen that the ThT fluorescence intensity of dsDNA with 2 or 3 CGG units is almost close to ploy$T(CGG)_{2/3}$, imply the double-chain and cavity formation is too limited to provide a better lighting. However, the 6H3M2 and 6H3M3 still show the significantly better fluorescence-enhancing capabilities than the double and single stranded conformation with the same number of CGG units, as well as the complementary hair-

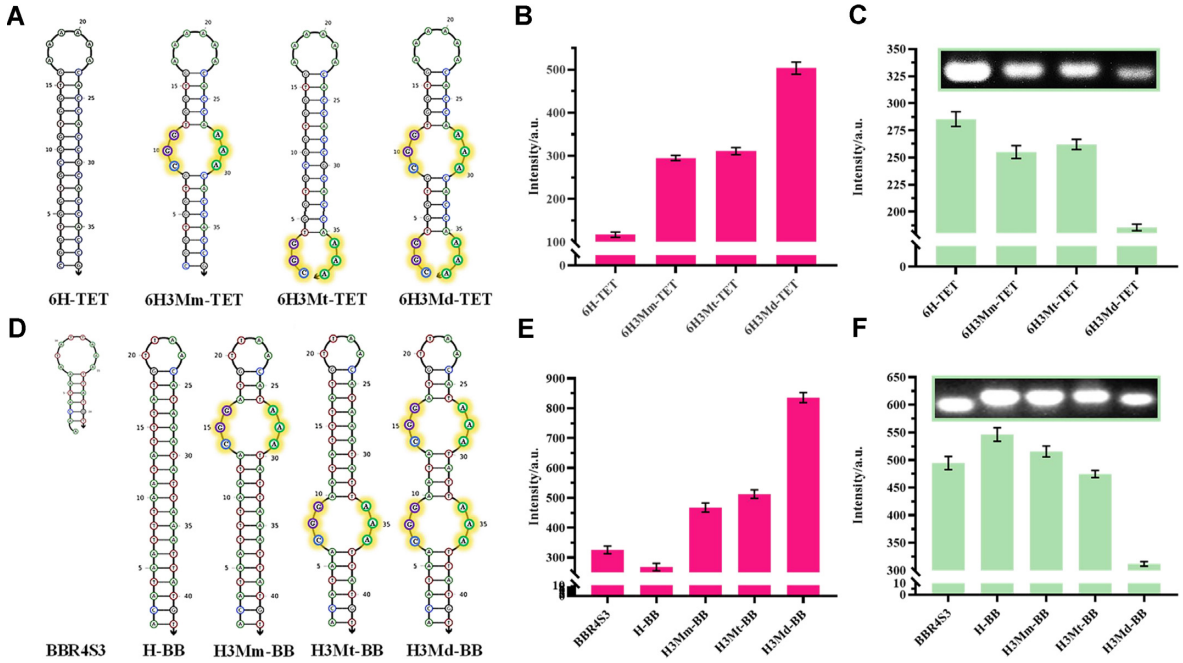

Figure 3. The assessment of CGG-AAA cavity structure lighting ThT at nucleic acid sequence with actual functional. The predicted secondary structure of the (**A**) TET and (**D**) BB nucleic acid sequences with CGG-AAA cavities. The ThT excitation ability of the (**B**) TET and (**E**) BB nucleic acid sequences with CGG-AAA cavities. The changes in the SGI fluorescence intensity and electrophoretic bands of the (**C**) TET and (**F**) BB nucleic acid sequences with CGG-AAA cavities.

pin, although the sudden-dropped complementarity also happened to them and leading the lighting effects of them are not as good as 6H3M1. It is sufficient to reflect the value of CGG-AAA cavity and hairpin loop existence.

Thus, we have reason to believe that ThT fluorescence enable to be stronger excited than that of complementary duplex when binding to duplex containing CGG-AAA mismatched cavity, as long as the degree of complementarity between the duplex is ensured, which means control a moderate number of introduced-cavities.

Next, we expected to find a short ssDNA with actual functional whose sequence composition contains the basis for the CGG-AAA cavity formation, so as to verify its actual excitation effect on ThT. A 8 nt TET aptamer containing CGG cavity unit tailored by Kwon *et al.* (37) was finally focused by us. Of note, it is also a G-rich sequence for ThT lighting, and a 16 nt bivalent aptamer had been proposed to facilitate the formation of G4 on this basis (38). Thus, the complementary duplexes, complementary duplex hairpins, and sequences with mismatched bases introduced for cavity formation was designed in our study (Supplementary Table S1) (Supplementary Figure S2A), so that not only the actual existence value of CGG-AAA mismatch can be evaluated, but also the fluorescent excitation effect of G4 and cavity on ThT can be compared.

From the results in Supplementary Figure S2B and C, we can see that the best ThT lighting and the duplex formation both came from the hairpin bivalent aptamer (6H-TET), which confirms once again our previous inference that the hairpin loop can better pair the double chains with complementary potential to form a duplex and enhance ThT fluorescent.

Since the sequences of 6H-TET contains two repeat CGG units, we first explored the location and numbers influence of CGG-AAA cavity on ThT excitation (Figure 3A). As shown in Figure 3B and C, the hairpins with single cavity in the middle (6H3Mm-TET) or tail (6H3Md-TET) has similar levels of ThT fluorescence emission and the degree of duplex complementarity, suggesting the cavity location does not unduly interfere with the ThT lighting as long as the complementarity of the duplexes does not change significantly. For the double cavities (6H3Md-TET), it can be seen that although the degree of complementarity will be affected slightly, it still can achieve a nearly 17 times than B-TET, 5 times than 6H-TET, and 1.7 times than hairpins with single cavity for ThT lighting, proving the presence of CGG-AAA mismatched cavity at hairpin arm can effectively light up ThT, even much more than the single-stranded with potential to form G4.

Moreover, to better verify the universality of cavity, we designed another hairpin with CGG-AAA cavity containing BB fluorescent aptamer sequence (39) with the basic cavity base unit AAA (Supplementary Table S1) (Figure 3D) by using the similar way of 6H3Md-TET constructing. In good agreement with above results (Figure 3E, F), H3Md-BB exhibits higher efficacy on ThT lighting.

CHTLNAS-based TET aptasensor

Introducing a CGG-AAA mismatch into a duplex exhibits the potential for CHTLNAS developing into a fluorescence turn-off sensor, especially the the 6H3Md-TET sequence is designed for cavity hairpin verification, as well as the bivalent aptamer may enhance the sensor response rate (40).

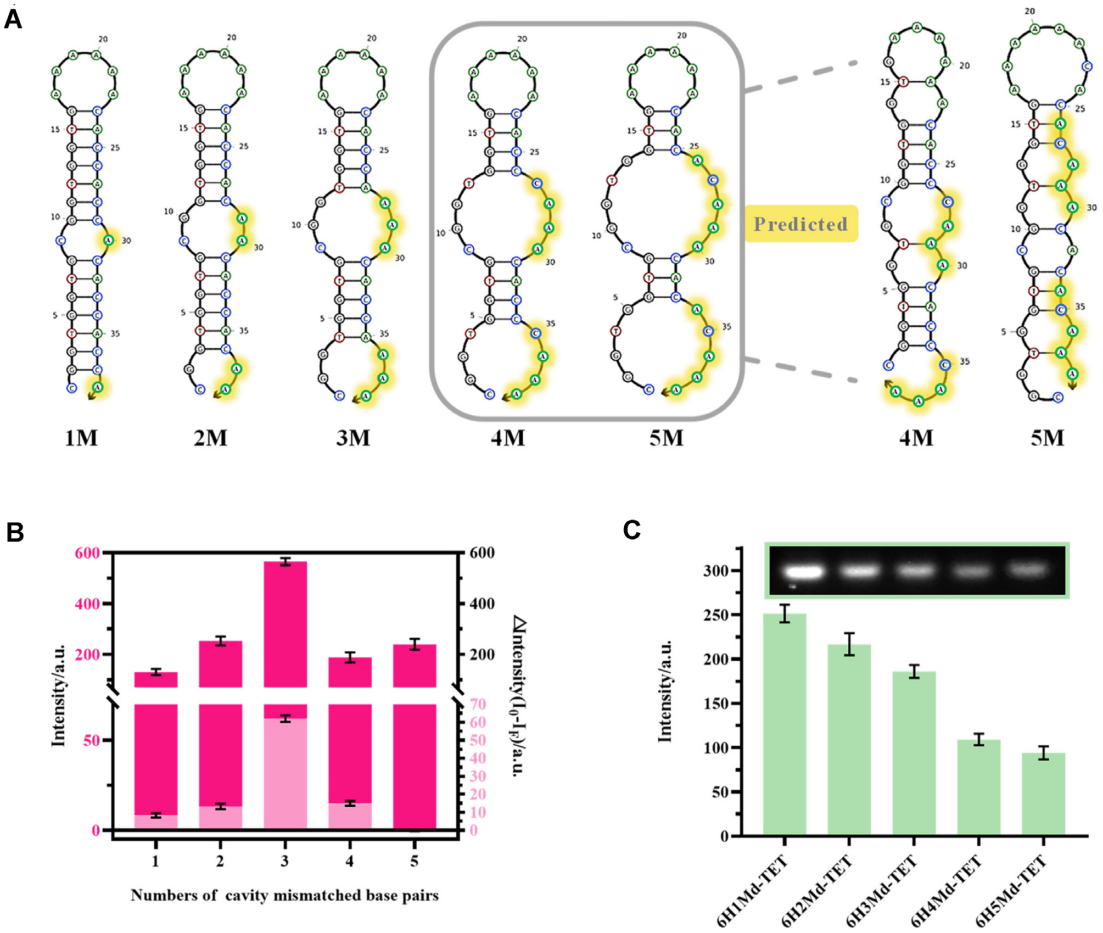

Figure 4. The feasibility of the cavity hairpin for TET detection. (**A**) The expected and predicted secondary structure of the hairpin with different degrees of complementarity. (**B**) The ThT excitation ability (dark pink bars) and fluorescence difference before and after responding to the TET (light pink bar) in the TET-hairpin with mismatched base pairs. (**C**) The SGI fluorescence intensity and electrophoretic band changes in the TET-hairpin with increased mismatched base pairs.

Moreover, considering that the performance of the fluorescence aptasensor is inextricably related to the rapid and sensitive structural response, it is speculated that the target typically cannot compete with duplex formation if a full-length complementary hairpin arm is employed, making it difficult to induce conformational changes and output detection signals. It is hypothesized that the cavity hairpin may be more successful in meeting the precise sensing needs due to the presence of mismatched base pairs (41,42). To demonstrate this on the basis of retaining CGG-AAA mismatch formation, the bases at the 3′-end of the bivalent aptamer complementary chain were replaced with 1–5 A or C bases at corresponding positions to construct a hairpin with different degrees of complementarity, containing cavities of different sizes (Supplementary Table S1) (Figure 4A). Then, the hairpin structure responsible for the most significant TET to opening and strongest differential ThT signal changes were examined. As shown in Figure 4B, 6H3Md-TET showed the optimal effect. The hairpins were characterized via fluorescence and agarose electrophoresis to clarify this issue(Figure 4C), the SG1 emission peak decreased gradually with mismatched base pairs from 1 to 5. In particular, the fluorescence displayed a distinct decline when the mismatched base pairs exceeded 3, while the corresponding brightness of the gel electrophoresis channel darkened significantly, indicating that 6H4Md-TET and 6H5Md-TET failed to form a stable hairpin structure to provide the fluorescence response caused by its own structural change for ThT before and after target addition.

The ThT fluorescence results showed that 6H3Md-TET was enhanced the most among the hairpin group with different degrees of complementarity in the absence of a target. Furthermore, the ability of the cavity hairpins to light up ThT increased after replacing the 1–3 A bases (Figure 4B). Analysis of the secondary conformations indicated that the G-A mismatched pair increased gradually in the cavity formed by the hairpins, while the C-A mismatch remained unchanged, confirming the proposed theory of cavity-enhanced ThT. Additionally, the secondary conformations of 6H4Md-TET and 6H5Md-TET displayed substantial changes due to the introduction of additional unpaired bases (Figure 4A). However, this did not contradict the analysis above. The duplex formation was still weakened due to the limited number of complementary base pairs, explaining why 6H4Md-TET and 6H5Md-TET did not further enhance ThT emission with a G-A mismatch

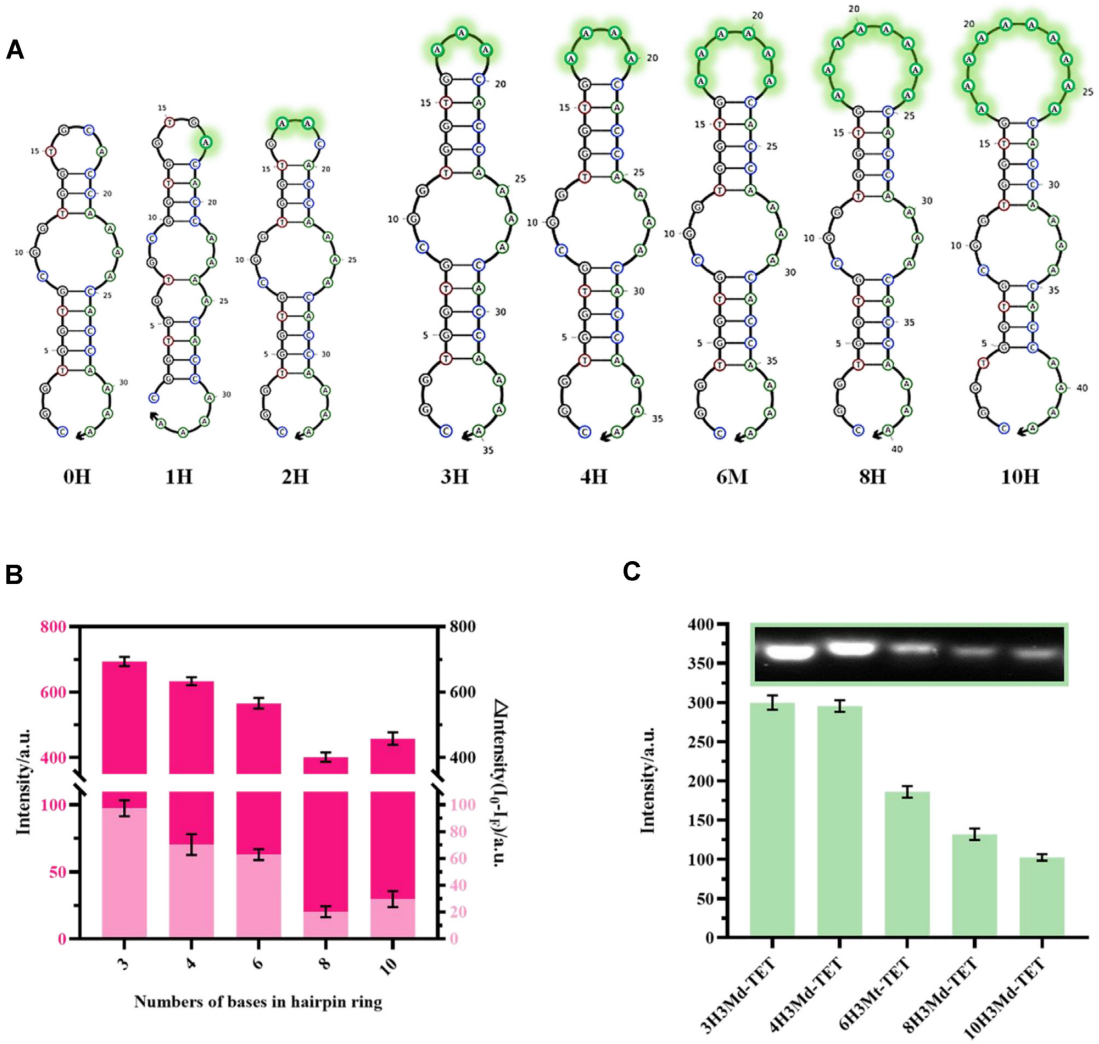

Figure 5. Optimization of the base number of the hairpin loop for TET detection. (**A**) The predicted secondary structure of the hairpins. The green marker represents the added bases for loop formation. (**B**) The ThT excitation ability (dark pink bars) and the fluorescence difference before and after responding to the TET (light pink bar) in hairpins. (**C**) The SGI fluorescence intensity and electrophoretic band changes in hairpins.

increase. Therefore, 6H3Md-TET maintained the optimal conformational balance between the structural stability of the hairpin and the ease with which the target could facilitate changes, as well as CGG-AAA cavity formation, in this case, contributing to a maximum difference in the signal output ability. Thus, 6H3Md-TET allows to serve as a promising CHTLNAS for subsequent optimization.

Elucidation of the CHTLNAS mechanism in the previous section indicated that the introduction of the loop connecting the hairpin arm promoted complementary duplex pairing via positional proximity. Therefore, this study first attempted to optimize the number of bases in the loop to explore the optimal closure of the hairpin, which improved the fluorescence emission without a target, reduced the background signal during analysis, and met the detection sensitivity requirements. Predicting the secondary structures of the hairpins in the loop with a varying number of bases and ensure the consistency of the complementary hairpin base pairs and CGG-AAA cavity conformations. The secondary structure of the hairpin with 0-base to 2-base loop intervention was completely different (Figure 5A). Therefore, we started to synthesize the hairpin which loop with 3 bases and carried out subsequent verification. In the absence of TET, an obvious decline in SGI fluorescence when the number of loop bases increased to 6 (Figure 5C), indicating that the closed stability of the hairpins containing loops with 3 or 4 bases could be optimally maintained. Accordingly, 3H3Md-TET displayed a more significant ThT enhancement and an intensity change after TET added, although 10H3Md-TET showed better ThT enhancement and detection potential than 8H3Md-TET (Figure 5B), it might benefit from the promotional effect of the A base in the hairpin loop, resulting in a rebound of the ThT fluorescence.

The 3H3Md-TET was employed as a CHTLNAS to establish the TET aptasensor. The impact of several critical factors and key parameters were investigated to optimize the label-free aptasensor conditions.

First, the optimum intercalating time of ThT into the cavity of 3H3Md-TET was measured according to the fluorescence kinetics curve changes in ThT at 0.02 s intervals after

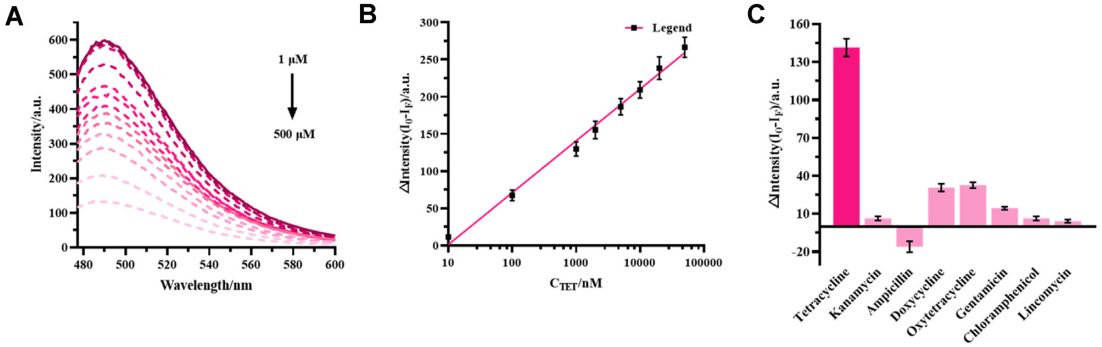

Figure. 6. The detection capability evaluation of the CHTLNAS-based TET aptasensor. (**A**) The fluorescence spectra of the ThT incubated with different concentrations of TET. The solid line represents the ThT fluorescence curve in the absence of TET. (**B**) The linear calibration of the decreased fluorescence intensity (I_0 - I_F) versus the TET concentration. (**C**) The histograms of the TET analogs for the selectivity tests. Each concentration of the additional antibiotics was 12.5 μmol l^{-1}, while the TET concentration was 1.25 μmol l^{-1}. The error bars illustrate the standard deviations of three replicate measurements.

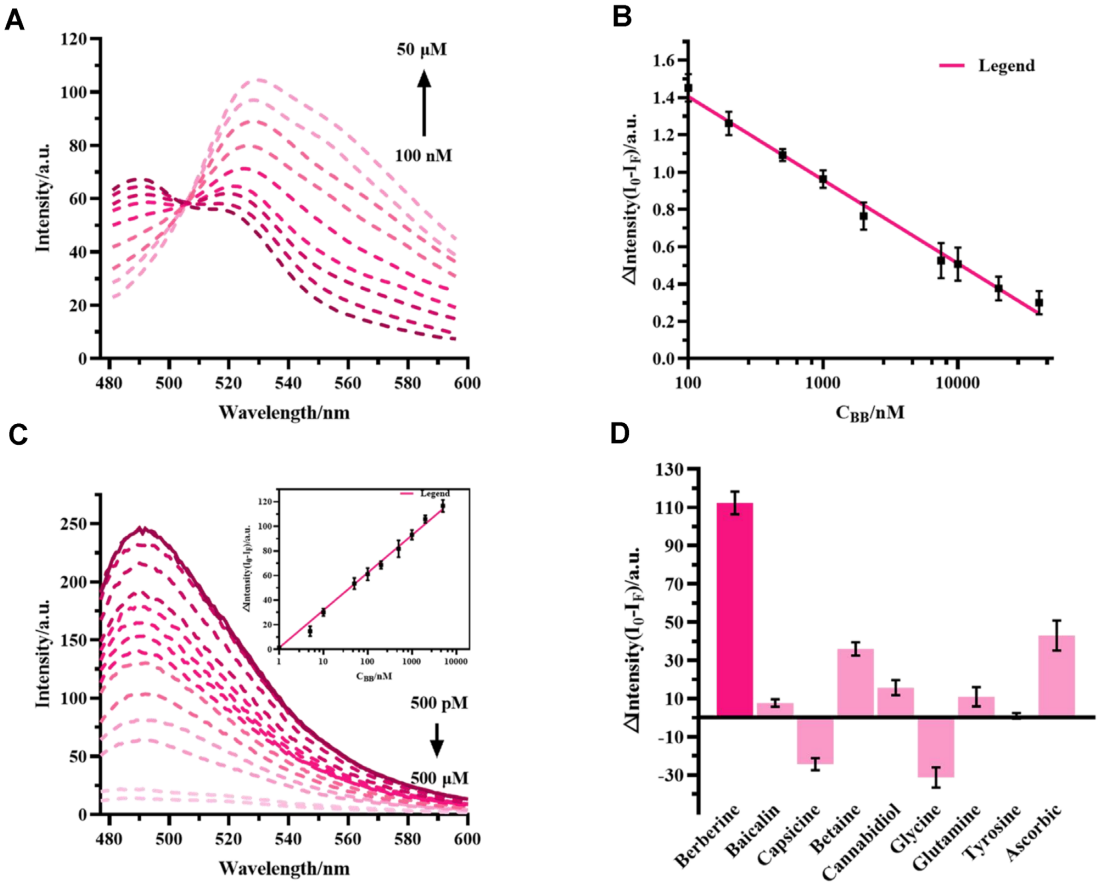

Figure 7. The detection capability evaluation of the CHTLNAS-based BB aptasensor. (**A**) The fluorescence spectra of the system in the presence of various BB concentrations. (**B**) The linear calibration of the changed fluorescence intensity (I_{490}/I_{530}) versus the BB concentration. (**C**) The fluorescence spectra of the ThT incubated with different BB concentrations. The solid line represents the ThT fluorescence curve in the absence of BB. Insert figure: The linear calibration of the decreased fluorescence intensity (I_0–I_F) versus BB concentration. (**D**) The histograms of the BB analogs for the selectivity tests. Each concentration of the additional antibiotics was 12.5 μmol l^{-1}, while the TET concentration was 1.25 μmol l^{-1}. The error bars illustrate the standard deviations of three replicate measurements.

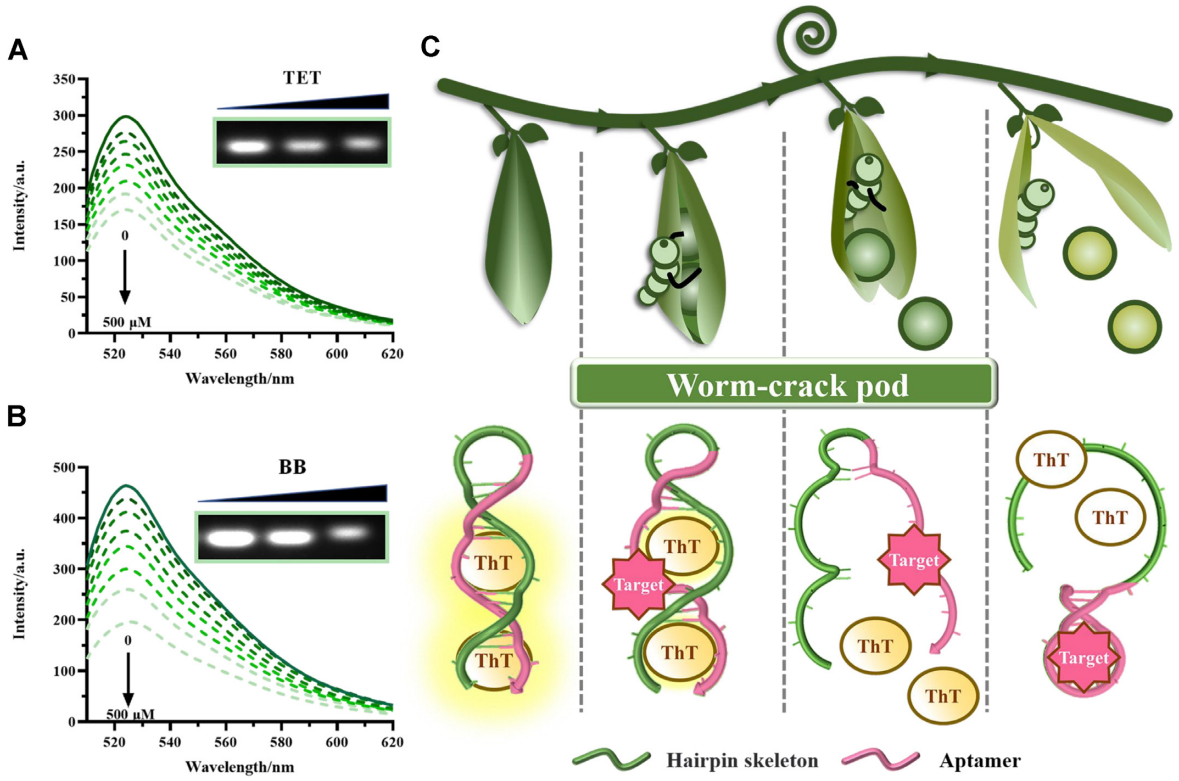

Figure 8. The *Worm-crack pod* mechanism of the CHTLNAS mediated by targets. The (**A**) 3H3Md-TET and (**B**) H3Md-BB fluorescence results of the SYBR Green I and gel retardation assays, with the change in the TET/BB concentration. The initial trace is depicted by the solid line in the absence of a target, while the dashed traces depict changes in the SYBR Green I emission peaks after the addition of TET/BB up to 500 μM. (**C**) The *Worm-crack pod* schematic of the ligand-mediated ThT displacement in CHTLNAS.

vortex mixing with the sequences. As shown in Supplementary Figure S3A, the fluorescence intensity of ThT continued to rise after introduction into the reaction medium, with no obvious changes observed after 5 min, indicating that the ThT could rapidly bind with the hairpin.

Subsequently, the optimum incubation time of TET with 3H3Md-TET indicated by the ThT fluorescence change curve was analyzed (Supplementary Figure S3B). The fluorescence decreased rapidly after adding TET to the reaction solution, while two consecutive small peaks were observed during the first 30 s (Supplementary Figure S3B insert), indicating competition between the open TET hairpin structure destroying the cavity conformation and ThT binding with the cavity for fluorescence excitation. The curve remained constant after 8 min, which was selected as the optimal reaction time between the TET and the sequence.

Since the appropriate ThT to nucleic acid sequence ratio is critical for ensuring assay sensitivity, the 3H3Md-TET concentration was fixed at 1 μM while different concentration of ThT was set in gradient experimental groups. The results are shown in Supplementary Figure S3C, the fluorescence intensity was first increases with increasing ratio of $C_{sequence}$:C_{ThT} from 10:1 to 1:2, and decreased afterwards, which indicated that the ThT molecules tended to form dimers or polymers at high concentrations, which was constrained by the molecular structure and size (43), failing to match well with the cavity in the hairpin and facilitate emission. Suggesting that the ThT fluorescence response to the sequence reached saturation, and 1:2 is the optimal ratio for subsequent experiments.

Finally, the influence of the reaction buffer on the system was explored. As shown in Supplementary Figure S3D, the fluorescence intensity changes in the presence of TET in Tris-HCl (pH 7.4) were more significant than in other ion buffering systems, exhibiting a maximum △Intensity of ThT in 10 mM Tris-HCl, providing a suitable buffer environment for the aptasensor to realize conformational free transformation (13).

The detection performance of 3H3Md-TET was explored in optimal experimental conditions by analyzing different TET concentrations (Figure 6A). In the absence of TET, the reaction system displayed the strongest ThT fluorescence. After adding TET, the fluorescence intensity decreased as the TET concentration increased, exhibiting a good linear relationship ($Y = 65.26516 \log X – 54.5016$, $R^2 = 0.99526$) between the logarithm of the TET concentration from 1 nM–50 μM and the fluorescence difference ($I_0 – I_F$) before and after TET addition (Figure 6B), with a LOD of 0.64 nM.

To evaluate the specificity of this sensor, different antibiotics (44) (kanamycin, ampicillin, doxycycline, oxytetracycline, gentamicin, chloramphenicol, and lincomycin) were choose to serve as the interfering substances to perform parallel measurements. As shown in Figure 6C, the TET analogs did not significantly interfere with the detection, in-

dicating a good selectivity of the developed TET aptasensor. The doxycycline and oxytetracycline occured a relatively obvious fluorescence change, which may be attributed to the similar binding sites between the aptamer and TET (37).

The applicability and reliability of the TET sensor were tested in real sample detection. By substituting the fluorescence difference at 490 nm into the standard curve, the relationship between the actual addition concentration and the recovery concentration was obtained, ranging from 98.6 %–105.8 % (Supplementary Table S2), further confirming the ability of the sensor to rapidly detect TET in actual samples.

As a universal antibiotic, diversified label-free sensors for detecting TET based on DNA have been continuously proposed (Supplementary Table S4). Based on the different signal reporting, methods can be mainly classified as colorimetric, electrochemical and fluorescence. For the colorimetric sensors, it mainly catalyzes the color reaction to achieve detection by mediating the formation of special structure DNAzyme, such as G4. However, the performance of DNAzymes and the sufficient coloration require harsh conditions and longer reaction time, and even some nucleic acid amplifications were introduced to support signal sensitization (45,46), which may result non-specific amplification reaction, reducing the detection accuracy. For electrochemical sensors, the sensing interface modifies the aptamer to complete the electrical signal changes before and after capturing TET, which better ensure the sensitivity of sensors, but the preparation process is too cumbersome and time-consuming, as well as requiring the operator to be highly professional. In comparison, the fluorescence sensor, which uses nucleic acids as allosteric molecules to guide the change of specific molecular signal, is more suitable for TET POCT in food safety application, because the system is simpler, the cost is lower and the signal report is faster. Especially for the label-free sensor, its sensitivity is mainly determined by the selected fluorescent reporter molecule and the matching sensing principle. Compared with the same-type-detection previous studies with the same signal reporter molecules(47,48), our senor is undoubtedly the most excellent in sensing sensitivity and time using, as well as allows a wide liner range, which fully meet the detection of the maximum residue standard of TET with 225 nM allowable by the European Union (49). Moreover, without any organic components, integrating detection and output, our sensor simplifies the experimental process and cost, effectively ensure the health of operators.

CHTLNAS-based BB aptasensor

The excellent TET detection performance of CHTLNAS prompted this study to develop a BB aptasensor. Since the number of bridging bases constituting the hairpin loop affects the complementarity of the hairpin arms and thus the sensor's sensitivity, it is necessary to make sure the number of the bridging bases. Further, from the aforementioned optimization of TET aptasensor, the verified bases number for hairpin loop is three, while in the design of CHTLNAS for BB detecting, it was found that the secondary structure of H3Md-BB already had two base pairs at the hairpin loop that could not complement properly before any additional bridging bases were added (Figure 3D). Therefore, considering the complementary stability of the hairpin and the flexibility of mediating conformational changes after BB addition, it was concluded that the conformation of H3Md-BB was already maximally close to the optimal conformational conditions of the sensor and no further introduction of bridging bases was needed to avoid affecting the sensitivity of the fluorescence reaction.

Considering H3Md-BB contains BB fluorescence aptamer sequence, we endeavored to construct a BB ratiometric fluorescence aptasensor. As shown in Supplementary Figure S4, BB and ThT show a good fluorescence emission at their optimum excitation wavelengths (365 nm/445 nm), respectively, while the intensity of both is very weak when exchanging excitation wavelengths, especially for BB. Therefore, ignoring the fluorescence effect of BB fluorescence on ThT at the excitation wavelength of 445 nM, the optimization form same to 3H3Md-TET for BB sensor were carried and showed in Supplementary Figure S5.

On the basis of ensuring the consistency of reaction conditions, we reduced the concentration of ThT to 100 nM and finally obtained the expected clear double-peak fluorescence change curve at 445 nm excitation wavelength (Figure 7A). It can be seen that with the increase of BB concentration, the fluorescence emission peak of ThT at 490 nm decreases and the BB fluorescence emission peak at 530 nm is enhanced, and the value of I_{490}/I_{530} gradually decreases, and there is an obvious linear relationship between the ratio and the logarithm of BB concentration between 100 nM–50 μM, and the linear regression equation is $Y = -0.44197 \log X + 2.28556$ ($R^2 = 0.99265$) (Figure 7B), with a LOD of 24.99 nM, showing the feasibility of constructing a label-free ratiometric fluorescent sensor based on H3Md-BB.However, the maximum emission peaks of ThT and BB were extremely close, as well as the BB emission peak showed an obvious blue shift with a decrease in the concentration, indicating that both fluorescence signals interfered with each other. In addition, the ThT concentration that had to be reduced to ensure the simultaneous appearance of the ratiometric dual peaks also weakened the signal response sensitivity to some extent, resulting a limited detection range. Therefore, considering the sensitivity of the fluorescence changes and the practicability of the detection, ThT was ultimately selected as the single signal output of the sensor. The sensing results in Figure 7C show that the fluorescence emission peak of ThT at 490 nm became weaker at a higher BB concentration. When the BB concentration reached 500 nM, the fluorescence curve flattened, indicating that the system detection ability was reaching saturation. A linear relationship between the fluorescence difference ($I_0 - I_F$) and BB concentration logarithm was obtained in a range of 1 nM–10 μM ($Y = 30.556 \log X + 1.467$, $R^2 = 0.99756$) (Figure 7C insert). The LOD was 0.55 nM, indicating the sensitive detection performance of the H3Md-BB aptasenor.

The selectivity of the CHTLNAS-based BB aptasensor was investigated (50,51). As shown in Figure 7D, natural products and bioactive substances which was ten times the BB concentration only yielded a weak response, suggesting the developed method for detecting BB was specific. The detection of the BB in plasma samples were analyzed and calculated according to the standard curve. The relationship

between the actual addition concentration and the recovery concentration was determined in a range of 104.7 %–106.4 % (Supplementary Table S3), confirming the reliability and practicality of this method.

Based on its own characteristics, berberine mostly acts as a fluorescent molecule in a label-free sensor to report the detection signal, while for its own detection, it still stays in the stage of relying on large-scale instruments, such as high-performance liquid chromatography (52), mass spectrometry (53) and capillary electrophoresis (54), although the accuracy is high, the analysis cost is expensive and cannot meet the needs of large-scale on-site detection. Even if some receptors of macrocyclic aromatic hydrocarbons, such as cucurbituril (55,56) and pyrene derivative (57), have been found enable to excite BB fluorescence and achieving sensing, their specificity and sensing ability cannot be directly proportional to its complex synthesis process (58). At present, a simpler and more portable DNA-mediated label-free BB sensor needs to be developed. Sheng *et al.* (51) realized a sensitive (0.3 nM) detection of BB in drugs by the turn-off fluorescence of aggregated AgNCs which mediated by the binding of BB to the natural fish sperm DNA(fsDNA). However, the fsDNA is not a BB aptamer, which means that any other small molecule may interact with DNA and interfere with the detection specificity. In addition, the linear range with 5–2000 nM can only measure in visual semi-quantitatively, the actual quantitative detection range is very limited. Therefore, the two label-free fluorescent BB sensors based on the CHTLANS proposed in this study undoubtedly achieved a breakthrough in terms of specificity, cost, testing time, and quantitative detection linearity range compared with the above, which truly improved the detection practicability, convenience and safety, made up for the gap in the construction of aptamer-based BB sensors.

The *worm-crack pod* mechanism of CHTLNAS mediated by targets

The sensitive signal responsiveness of the CHTLNAS-based TET/BB aptasensor benefit from its own flexible allosteric effect on the target. To test this hypothesis, it was monitored via SGI spectroscopy and gel electrophoresis (Figure 8A, B). The strongest fluorescence (solid black line) and brightest electrophoretic band both appeared in the absence of a target, indicating that the switch maintained a good hairpin structure. The addition of TET/BB caused maximum emission at 525 nm of the SGI, while the electrophoretic band lightness decline was target-dependent. This suggested that the hairpin arm complementarity difficulty increased with the addition of the target concentration, while the unstable pairing decreased the double-chain proportion in the secondary CHTLNAS structure, leading to an excessive transition from a stable hairpin double-chain structure to an open single-chain structure. This explains why the electrophoretic band cannot be clearly characterized by a double-chain indicator and why the change in the sequence migration speed decreases (the size effect).

To better illustrate the mechanism behind the target-mediated ThT displacement in CHTLNAS, this study labeled the process as a *Worm-crack pod.* As illustrated in Figure 8C, the CHTLNAS is compared to an immature pod, where green peas are trapped by the peel as ThT binds to the cavity. Then, peels cracking and peas falling down when worm crawls to peel the pods, as the similar process of the CHTLNAS conformation from closed to open after targets added for interfering the complementary trend between aptamer and hairpin arm, resulting ThT out of the cavity. Furthermore, the fallen peas turn from green to yellow as the worm occupies the bean pit, just like the gradual difficulty forming of CGG-AAA, accompanied by the turn-off of ThT lighting.

CHTLNAS facilitates the intracellular imaging of ThT and slows its nuclear entry

The excellent excitation effect of the hairpin with a cavity on ThT *in vitro* prompted this study to further confirm whether it can also light ThT in cells and realize intracellular imaging. We selected H3Md-BB (and H-BB sequence without cavity, acting as a control group) with functional sequence with better ThT excitation effect *in vitro* as a candidate CHTLNAS to verify. Both sequences with good thermal stability (The fluorescence decreased to 97 %/89 % and 50 % of the initial value at 37.00 °C and 63.85 °C/58.66 °C, respectively) in cell culture condition (37 °C) were first determined by melt temperature measuring (Supplementary Figure S6). The cholesterol-modified linker at the 3′-end of H3Md-BB (H3Md-BB-3′chol) (Supplementary Table S1) was conjugated to the surface of the synthesized liposomes (HC-Lip) (Supplementary Figure S7). The optimal ratio of phospholipids to nucleic acid (P/N) was determined as 500:1, which yielded the clearest and brightest electrophoretic bands retained in sample hole (Supplementary Figure S8), suggesting that the sequence was successfully modified onto the liposomes. Then, ThT was loaded onto HC-Lip to form HC-Lip+ThT, which was incubated with 3T3-L1 cells. As shown in Supplementary Figure S9, the ThT distribution was clearly evident in the cytoplasm of the HC-Lip+ThT transfected group (experimental group). However, when exposed to the same treatment, the fluorescence of the ThT in the H-Lip+ThT group (control group) was significantly lower than in the experimental group, suggesting that CHTLNAS could still facilitate excellent ThT excitation in the cells, again confirming the value of the presence of a cavity. Furthermore, the liposome signal (red) and ThT signal (green) displayed good co-localization in the cytoplasm, which was not observed in the control group. Moreover, a more pronounced dispersion trend was evident for ThT nuclear internalization in the control group, implying that the presence of a hairpin cavity could light up the ThT and allow more stable ThT loading than a complementary hairpin.

The UV-absorption spectral changes shown in Supplementary Figure S10 confirmed the prediction. The ThT displayed a characteristic absorption profile at a maximum of 412 nm without DNA, while the spectral changes in the TET, BB and AT non-functional hairpin groups were similar after adding the sequences. Although a bathochromic shift was evident in the ThT absorption band, the extent of the bathochromic complementary hairpin changes in each group was significantly less than the cavity hairpin. Mean-

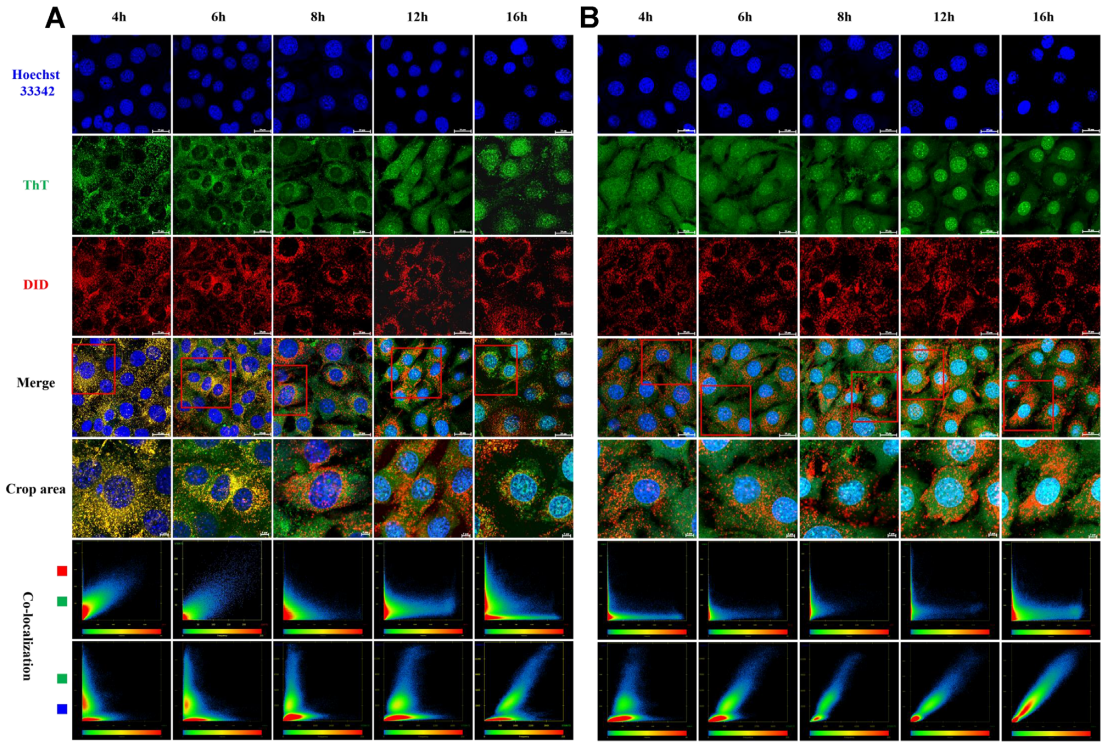

Figure 9. The CLSM images of the 3T3-L1 cells after incubation with (**A**) HC-Lip+ThT and (**B**) H-Lip+ThT for 4, 6, 8, 12 and 16 h, respectively. The liposomes were stained with DID dye (red), and the cell nucleus was stained with Hoechst33342 (blue). The pseudo color of the ThT channel was adjusted to green to enhance characterization and distinguish it from other channels. The scale bar of each image before crop is 20 μm, after crop is 5 μm.

while, the binding affinity of cavity hairpin to ThT was higher than complementary hairpin (Supplementary Figure S11), which indicating a successful, stable DNA-ThT complex formation for the cavity hairpin and stronger interaction between the ThT and the CGG-AAA cavity. Moreover, the ThT competition between hairpins with or without a cavity can be evaluated according to the real-time fluorescence changes. After ThT was added to the initial measuring system, no visible increase was apparent in the fluorescence intensity. However, under the phase of excessive ThT concentration, the fluorescence intensity gradually enhanced with the alternate addition of complementary and cavity hairpins (Supplementary Figures S12B–D). The addition of each cavity hairpin facilitated a more significant fluorescence increase than that of the previous complementary hairpin, demonstrating the superior excitation effect of the cavity on ThT. Subsequently, the excess ThT was gradually consumed as the total amount of nucleic acid in the system continued to increase. The fluorescence enhancement caused by adding hairpins became increasingly limited until the intensity no longer increased after complementary hairpin addition, indicating that the ThT was completely consumed. Furter, the first platform phase was broken by the subsequent addition of the cavity hairpin, gradually increasing the fluorescence until reaching the second platform phase. When in this stage, no changes were evident in the fluorescence regardless of the cavity or complementary hairpin added. However, the control group that received the addition of the same sequence from beginning to end displayed neither the differential rise in ThT intensity nor the second platform phase during the gradient fluorescence increase (Supplementary Figure S12A). This suggests that after the hairpin amount reaches the ThT lighting saturation point, the cavity hairpin exhibits a stronger competitive binding ability to ThT than the complementary hairpin, enable to rob ThT from complementary hairpin for binding with and enhance ThT excitation, resulting in a gradient rise of fluorescence.

According to above findings, we further evaluated the intracellular loading stability of the ThT carried by the cavity hairpin over time and stained the nucleus with Hoechst 33342 to better assess the nuclear entry of ThT. In addition, the excitation voltage of the ThT channel in the control group was increased to ensure that the results were compared with a baseline as close to the experimental group as possible.

As shown in Figure 9A, the liposome signal was detained in the cytoplasm throughout the process, indicating that the HC-Lip/H-Lip was not allowed to enter the nucleus. With the cellular uptake of HC-Lip+ThT, the ThT signal displayed obvious co-localization with the liposomes (yellow dots) within 8 h, verifying the conjecture that the cavity hairpin could load ThT. After this point, fewer yellow dots appeared in the cytoplasm, indicating that HC-Lip could no longer stably transport the ThT with the prolongation of cell entry. This phenomenon may be related to the degradation of the hairpin sequence caused by the presence of multiple nucleases in the cell (59). Contrarily, the red and green signal co-localization never occurred in the control group. The ThT signal was scattered throughout the cell region af-

ter 4 h transfection, indicating that the liposomes modified using a hairpin without a cavity had no significant promotional effect on ThT loading (Figure 9B).

Furthermore, with the extension of the cell-uptake time, the ThT was distributed throughout the cell and lit up the nuclear region, especially the nuclear spot. The highest green fluorescence intensity was evident in the experimental group after incubation for 16 h, while a cyan overlap by the green and blue signal was observed in the control group after transfection for only 8 h. This phenomenon can be attributed to the considerable number of nucleic acid sequences in the nuclear genome that can form G4s and others to light up ThT (60), causing the nucleus to become more attractive to ThT than the cytoplasm. Therefore, ThT gradually concentrates in the nucleus over time.

These changes were further confirmed by the quantitative analysis of Mander's overlap coefficients (*M*-value) (61,62). For the ThT and liposomes, the *M*-value of the experimental group showed a general downward trend but was maintained at more than 0.6 in 4–8 h. After 12 h, the *M*-value decreased rapidly to 0.3248 (12 h) and 0.2756 (16 h), gradually approaching the change values of the control group (Supplementary Figure S13A). As shown in Supplementary Figure S13B, the *M*-values of the ThT and cell nucleus increased in both groups. Before 8h, the experimental group increased slowly from 0.3109 (4 h) to 0.4200 (8 h), then began to rise rapidly until reaching 0.8302 (16 h). However, the *M*-value of the control group exceeded 0.50 after only 4 h, quickly reaching more than 0.8 at 12 h. These results suggested that the cavity hairpin could not only light up ThT but also stably load it after entering cells for a certain period. Therefore, the entry process of ThT into the nucleus and be nonspecific excitatied by unknown nucleic acid sequences could be effectively delayed. These results also indicated that cavity hairpins could aid ThT as intracellular tracers for delivery carriers such as liposomes, as well as can potentially address the situation that ThT can only passively localized in the nuclear region for imaging due to its own characteristics.

DISCUSSION

This study determined whether there is a mismatched cavity structure could be employed for binding and lighting ThT, which like bubbling that often appear in DNA processing, so as to improve the universality and practicality of NAC, and expand the application scenarios of ThT as a molecular fluorescent label. The docking of ThT with cavities hairpin mismatched from different pairs and types was simulated, showing that CGG-AAA cavity might provide an appropriate size and interaction force to restrict the two rotary aromatic rings in the excited state for ThT fluorescence exciting. Then, the conjecture was further validated from actual sequences, a fluorescence intensity over 500-fold higher than ThT spontaneous by CGG-AAA cavity hairpin, which cannot be realized for the fully complementary, providing a new mode for ThT lighting. Moreover, based on its flexible conformational responsiveness and sequence programmability, we designed CHTLNAS whose sequence containing TET or BB aptamer, and constructed three label-and enzyme-free fluorescent/ratiometric sensing platform after systematically optimization, achieving pM level detection of both targets in milk or plasma samples within 10 min. Of which, the sensitive fluorescence 'turn-down' changed of ThT was named as the worm-crack pod mechanism of CHTLNAS mediated by targets, enabling the construction of a universal aptasensors based on CHTLNAS.

Besides the excellent fluorescence excitation effect, the binding affinity (K_d ~2.938 μM) of CHTLNAS is much higher than that of the complementary duplex (K_d~159.6 μM). Meanwhile, compared to NACs (13,21,22,34) had been found to excite ThT fluorescence well (Supplementary Figure S14), although its affinity for ThT binding is slightly weaker than 22AG with different topologies induced under K^+/Na^+ conditions ($K_d(K^+)$~0.975 μM, $K_d(Na^+)$~1.978 μM), it still showed better binding affinity than ABA27 (K_d~20.53 μM), (GA)8-ps (K_d~14.26 μM), G Island ($dsDNA_{1+2}$) (K_d~26.47 μM), displaying good loading stability to ThT. Further, by modifying it onto liposomes, an intracellular tracer platform based on CHTLNAS was constructed to facilitate stable loading of ThT at low concentration levels (nM) and efficient imaging after cell entry, as well as prolong the loading time and slow down the attraction of high-concentrated nucleic acids in the nucleus, which under the condition without any additional chromogenic substances such as fluorescent labels or enzymes, and other delivery vehicles to assist in the ThT entry cells. It eliminates the complex operation, saves the amount of ThT, reduces its intracellular toxicity, as well as overcomes non-specific high background signal interference of ThT in the nuclear region, which is convenient for expanding the diversified application scenarios of ThT in the cell.

We also need to point out that, although there may be a better conformation than CGG-AAA for ThT excitation and even some conformations that can light up other fluorophores in the finite variety of possible cavity conformations formed by the arrangement and combination of different mismatched base pairs, the exploration method, research context, rational design of CHTLNAS, and its exploration process in the field of sensing and imaging in this paper are of great significance for future research.

The construction of a CGG-AAA mismatched cavity for ThT lighting shows potential for development into rich types of CHTLNAS or structural conversion components for analytical sensors *in vitro* and tracer imaging tools for intracellular delivery. Compared with the unconventional NACs like G4 reported for ThT lighting, the CHTLNAS with more unrestricted structure formation not only has good fluorescence excitation and loading stability for ThT, but also the allosteric flexibility and self-assembly potential of its hairpin structure deserves (63) attention to better serve as a signal change indicator, signal amplification or delivery tool in the field of ThT sensing, imaging, and the valuation of drug delivery and release kinetics. It will undoubtedly provide more inspiration for scientists in related fields by virtue of its more powerful application versatility, of which is also reflects the value of this study in exploring and designing the CHTLNAS based on mismatching.

DATA AVAILABILITY

The data underlying this article are available in the article and in its online supplementary material.

SUPPLEMENTARY DATA

Supplementary Data are available at NAR Online.

FUNDING

National Key Research and Development Program of China [2022YFF0607900]; National Natural Science Foundation of China [21927812]; Key Research and Development Program of Hebei Province [21372801D]; 2115 Talent Training Plan of China Agricultural University [00109012]; Young Elite Scientist Sponsorship Program by BAST [BYESS2022133]. Funding for open access charge: From our fundings.
Conflict of interest statement. None declared.

REFERENCES

1. Hobbs,J. and Morgan,A. (1963) Fluorescence microscopy with thioflavine-T in the diagnosis of amyloid. *J. Pathol. Bacteriol.*, **86**, 437–442.
2. Vassar,P., Culling,C. and Taylor,H. (1959) Amer Soc Investigative Pathology, Inc 428 east preston St, Baltimore, MS. *Am. J. Pathol.*, **35**, 718–718.
3. Naiki,H., Higuchi,K., Hosokawa,M. and Takeda,T. (1989) Fluorometric determination of amyloid fibrils in vitro using the fluorescent dye, thioflavine T. *Anal. Biochem.*, **177**, 244–249.
4. Naiki,H., Higuchi,K., Kitagawa,K., Shimada,A., Chen,W.-H., Hosokawa,M., Nakakuki,K. and Takeda,T. (1991) *Amyloid and Amyloidosis 1990*. Springer, pp. 393–396.
5. Blum,A. and Sohar,E. (1962) The diagnosis of amyloidosis: ancillary procedures. *Lancet North Am. Ed.*, **279**, 721–724.
6. Nordberg,A. (2004) PET imaging of amyloid in Alzheimer's disease. *Lancet Neurol.*, **3**, 519–527.
7. Fändrich,M., Fletcher,M.A. and Dobson,C.M. (2001) Amyloid fibrils from muscle myoglobin. *Nature*, **410**, 165–166.
8. Parker,C.A. and Joyce,T.A. (1973) Prompt and delayed fluorescence of some DNA adsorbates. *Photochem. Photobiol.*, **18**, 467–474.
9. Sugimoto,S., Arita-Morioka,K., Mizunoe,Y., Yamanaka,K. and Ogura,T. (2015) Thioflavin T as a fluorescence probe for monitoring RNA metabolism at molecular and cellular levels. *Nucleic Acids Res.*, **43**, e92.
10. Liu,X., Song,J., Wang,C., Yang,R., Sun,P., Huang,Y., Zhang,L. and Fan,Q. (2022) An amplified fluorescence biosensor for intracellular telomerase determination and in situ imaging based on thioflavin T and conjugated polymer nanoparticles. *Sens. Actuators B*, **371**, 132485.
11. Luo,X., Xue,B., Feng,G., Zhang,J., Lin,B., Zeng,P., Li,H., Yi,H., Zhang,X.-L., Zhu,H. *et al.* (2019) Lighting up the native viral RNA genome with a fluorogenic probe for the live-cell visualization of virus infection. *J. Am. Chem. Soc.*, **141**, 5182–5191.
12. Zhang,S., Sun,H., Wang,L., Liu,Y., Chen,H., Li,Q., Guan,A., Liu,M. and Tang,Y. (2018) Real-time monitoring of DNA G-quadruplexes in living cells with a small-molecule fluorescent probe. *Nucleic Acids Res.*, **46**, 7522–7532.
13. Mohanty,J., Barooah,N., Dhamodharan,V., Harikrishna,S., Pradeepkumar,P. and Bhasikuttan,A.C. (2013) Thioflavin T as an efficient inducer and selective fluorescent sensor for the human telomeric G-quadruplex DNA. *J. Am. Chem. Soc.*, **135**, 367–376.
14. Amdursky,N., Erez,Y. and Huppert,D. (2012) Molecular rotors: what lies behind the high sensitivity of the thioflavin-T fluorescent marker. *Acc. Chem. Res.*, **45**, 1548–1557.
15. Stsiapura,V.I., Maskevich,A.A., Kuzmitsky,V.A., Uversky,V.N., Kuznetsova,I.M. and Turoverov,K.K. (2008) Thioflavin T as a molecular rotor: fluorescent properties of Thioflavin T in solvents with different viscosity. *J. Phys. Chem. B*, **112**, 15893–15902.
16. Xu,S., Li,Q., Xiang,J., Yang,Q., Sun,H., Guan,A., Wang,L., Liu,Y., Yu,L., Shi,Y. *et al.* (2016) Thioflavin T as an efficient fluorescence sensor for selective recognition of RNA G-quadruplexes. *Sci. Rep.*, **6**, 24793.
17. Khusbu,F.Y., Zhou,X., Chen,H., Ma,C. and Wang,K. (2018) Thioflavin T as a fluorescence probe for biosensing applications. *TrAC Trends Anal. Chem.*, **109**, 1–18.
18. Faverie,R., Guédin,A., Bedrat,A., Yatsunyk,LA. and Mergny,J.-L. (2014) Thioflavin T as a fluorescence light-up probe for G4 formation. *Nucleic Acids Res.*, **42**, e65–e65.
19. Zhou,H., Wu,Z.-F., Han,Q.-J., Zhong,H.-M., Peng,J.-B., Li,X. and Fan,X.-L. (2018) Stable and label-free fluorescent probe based on G-triplex DNA and thioflavin T. *Anal. Chem.*, **90**, 3220–3226.
20. Lee,I.J., Patil,S.P., Fhayli,K., Alsaiari,S. and Khashab,N.M. (2015) Probing structural changes of self assembled i-motif DNA. *Chem. Commun. (Camb.)*, **51**, 3747–3749.
21. Liu,S., Peng,P., Wang,H., Shi,L. and Li,T. (2017) Thioflavin T binds dimeric parallel-stranded GA-containing non-G-quadruplex dnas: a general approach to lighting up double-stranded scaffolds. *Nucleic Acids Res.*, **45**, 12080–12089.
22. Zhou,W., Yu,Z., Ma,G., Jin,T., Li,Y., Fan,L. and Li,X. (2019) Thioflavin T specifically brightening "Guanine Island" in duplex-DNA: a novel fluorescent probe for single-nucleotide mutation. *Analyst*, **144**, 2284–2290.
23. Pramanik,S., Nandy,A., Chakraborty,S., Pramanik,U., Nandi,S. and Mukherjee,S. (2020) Preferential binding of thioflavin T to AT-rich DNA: white light emission through intramolecular förster resonance energy transfer. *J. Phys. Chem. Lett.*, **11**, 2436–2442.
24. Zhu,J., Yan,Z., Zhou,W., Liu,C., Wang,J. and Wang,E. (2018) Lighting up the thioflavin T by parallel-stranded TG(GA)n DNA homoduplexes. *ACS Sens.*, **3**, 1118–1125.
25. Verma,S., Ravichandiran,V. and Ranjan,N. (2021) Beyond amyloid proteins: thioflavin T in nucleic acid recognition. *Biochimie*, **190**, 111–123.
26. Liu,L., Shao,Y., Peng,J., Liu,H. and Zhang,L. (2013) Selective recognition of ds-DNA cavities by a molecular rotor: switched fluorescence of thioflavin T. *Mol. Biosyst.*, **9**, 2512–2519.
27. Zeida,A., Machado,M.R., Dans,P.D. and Pantano,S. (2012) Breathing, bubbling, and bending: DNA flexibility from multimicrosecond simulations. *Phys. Rev. E*, **86**, 021903.
28. Ping,H., Zhang,M., Li,H., Li,S., Chen,Q., Sun,C. and Zhang,T. (2012) Visual detection of melamine in raw milk by label-free silver nanoparticles. *Food Control*, **23**, 191–197.
29. Hu,Z., Xie,M., Yang,D., Chen,D., Jian,J., Li,H., Yuan,K., Jiang,Z. and Zhou,H. (2017) A simple, fast, and sensitive colorimetric assay for visual detection of berberine in human plasma by NaHSO 4-optimized gold nanoparticles. *RSC Adv.*, **7**, 34746–34754.
30. Ilanchelian,M. and Ramaraj,R. (2004) Emission of thioflavin T and its control in the presence of DNA. *J. Photochem. Photobiol. A*, **162**, 129–137.
31. Yan,Y., Zhang,D., Zhou,P., Li,B. and Huang,S.Y. (2017) HDOCK: a web server for protein-protein and protein-DNA/RNA docking based on a hybrid strategy. *Nucleic Acids Res.*, **45**, W365–W373.
32. Pramanik,S., Khamari,L. and Mukherjee,S. (2021) Differentiating a least-stable single nucleotide mismatch in DNA via metal ion-mediated base pairing and using thioflavin T as an extrinsic fluorophore. *J. Phys. Chem. Lett.*, **12**, 2547–2554.
33. Oliveira,L.M., Long,A.S., Brown,T., Fox,K.R. and Weber,G. (2020) Melting temperature measurement and mesoscopic evaluation of single, double and triple DNA mismatches. *Chem. Sci.*, **11**, 8273–8287.
34. Wang,H., Peng,P., Liu,S. and Li,T. (2016) Thioflavin T behaves as an efficient fluorescent ligand for label-free ATP aptasensor. *Anal. Bioanal.Chem.*, **408**, 7927–7934.
35. Zipper,H., Brunner,H., Bernhagen,J. and Vitzthum,F. (2004) Investigations on DNA intercalation and surface binding by SYBR Green I, its structure determination and methodological implications. *Nucleic Acids Res.*, **32**, E103–E103.
36. Skeidsvoll,J. and Ueland,P.M. (1995) Analysis of double-stranded DNA by capillary electrophoresis with laser-induced fluorescence detection using the monomeric dye SYBR green I. *Anal. Biochem.*, **231**, 359–365.
37. Kwon,Y.S., Ahmad Raston,N.H. and Gu,M.B. (2014) An ultra-sensitive colorimetric detection of tetracyclines using the

shortest aptamer with highly enhanced affinity. *Chem. Commun. (Camb.)*, **50**, 40–42.
38. Lan,X., Liu,N., Zhu,L., Chen,X., Chu,H., Li,X., Duan,N. and Xu,W. (2022) Tetracycline bivalent aptamer non-enzyme label-free sensor. *Shengwu Jishu Tongbao*, **38**, 276.
39. Wang,J., Zhang,Y., Wang,H., Chen,Y., Xu,L., Gao,T. and Pei,R. (2016) Selection and analysis of DNA aptamers to berberine to develop a label-free light-up fluorescent probe. *New J. Chem.*, **40**, 9768–9773.
40. Zhang,Z., Tao,C., Yin,J., Wang,Y. and Li,Y. (2018) Enhancing the response rate of strand displacement-based electrochemical aptamer sensors using bivalent binding aptamer-cDNA probes. *Biosens. Bioelectron.*, **103**, 39–44.
41. Deore,P.S., Gray,M.D., Chung,A.J. and Manderville,R.A. (2019) Ligand-induced G-quadruplex polymorphism: a DNA nanodevice for label-free aptasensor platforms. *J. Am. Chem. Soc.*, **141**, 14288–14297.
42. Phan,A.T. and Mergny,J.L. (2002) Human telomeric DNA: g-quadruplex, i-motif and Watson–Crick double helix. *Nucleic Acids Res.*, **30**, 4618–4625.
43. Biancardi,A., Biver,T., Burgalassi,A., Mattonai,M., Secco,F. and Venturini,M. (2014) Mechanistic aspects of thioflavin-T self-aggregation and DNA binding: evidence for dimer attack on DNA grooves. *Phys. Chem. Chem. Phys.*, **16**, 20061–20072.
44. Daghrir,R. and Drogui,P. (2013) Tetracycline antibiotics in the environment: a review. *Environ. Chem. Lett.*, **11**, 209–227.
45. Gong,X., Li,X., Qing,T., Zhang,P. and Feng,B. (2019) Amplified colorimetric detection of tetracycline based on an enzyme-linked aptamer assay with multivalent HRP-mimicking dnazyme. *Analyst*, **144**, 1948–1954.
46. Zhipeng,Z., Yao,T., Pengcheng,H. and Fang-Ying,W. (2020) Using target-specific aptamers to enhance the peroxidase-like activity of gold nanoclusters for colorimetric detection of tetracycline antibiotics. *Talanta*, **208**, 120342.
47. Dai,Y., Zhang,Y., Liao,W., Wang,W. and Wu,L. (2020) G-quadruplex specific thioflavin T-based label-free fluorescence aptasensor for rapid detection of tetracycline. *Spectrochim. Acta Part A*, **238**, 118406.
48. Chen,T., Ning,F., Liu,H., Wu,K., Li,W. and Ma,C. (2017) Label-free fluorescent strategy for sensitive detection of tetracycline based on triple-helix molecular switch and G-quadruplex. *Chin. Chem. Lett.*, **28**, 1380–1384.
49. Mohammad-Razdari,A., Ghasemi-Varnamkhasti,M., Rostami,S., Izadi,Z. and Ensafi,A.A. (2021) Magnetic and gold nanocomposite as a novel aptasensor for early detection of tetracycline residues. *J. Food Meas. Character.*, **15**, 3387–3396.
50. Wang,J., Sakthivel,R., Anbazhagan,R., Kubendhiran,S., Lai,J., Tsai,H. and Chen,S. (2020) Electroactive polypyrrole-molybdenum disulfide nanocomposite for ultrasensitive detection of berberine in rat plasma. *Anal. Chim. Acta*, **1125**, 210–219.
51. Sheng,L., Yangfang,K., Fangfang,M., Shu,C. and Yunfei,L. (2016) A sensitive spectrofluorometric method for detection of berberine hydrochloride using Ag nanoclusters directed by natural fish sperm DNA. *Biosens. Bioelectron.*, **85**, 758–763.
52. Li,P., Wang,T., Lei,F., Tang,P., Tan,X., Liu,Z. and Shen,L. (2014) Rosin-based molecularly imprinted polymers as the stationary phase in high-performance liquid chromatography for selective separation of berberine hydrochloride. *Polym. Int.*, **63**, 1699–1706.
53. Li,G., Yang,F., Liu,M., Su,X., Zhao,M. and Zhao,L. (2016) Development and application of a UPLC-MS/MS method for simultaneous determination of fenofibric acid and berberine in rat plasma: application to the drug–drug pharmacokinetic interaction study of fenofibrate combined with berberine after oral administration in rats. *Biomed. Chromatogr.*, **30**, 1075–1082.
54. Wen,A., Peng,X., Zhang,P., Long,Y., Gong,H., Xie,Q., Yue,M. and Chen,S. (2018) Spectrofluorometric determination of berberine using a novel Au nanocluster with large stokes shift. *Anal. Bioanal.Chem.*, **410**, 6489–6495.
55. Megyesi,M., Biczók,L. and Jablonkai,I. (2008) Highly sensitive fluorescence response to inclusion complex formation of berberine alkaloid with cucurbit[7]uril. *J. Phys. Chem. C*, **112**, 3410–3416.
56. Miskolczy,Z. and Biczók,L. (2014) Kinetics and thermodynamics of Berberine inclusion in Cucurbit[7]uril. *J. Phys. Chem. B*, **118**, 2499–2505.
57. Guo,M., Li,W., Sun,Y., Xu,H., Fan,Y., Ma,L., Huang,K. and Yao,Z. (2019) Rapid and visual detection of berberine hydrochloride based on a water-soluble pyrene derivative. *Luminescence*, **34**, 558–562.
58. Liu,C., Li,Z., Yu,H., Cui,N., Liao,X., Zhang,H., Shu,Z. and Yang,P. (2021) Host-guest co-assembly triggered turn-on and ratiometric sensing of berberine and its detoxicating. *Chin. Chem. Lett.*, **32**, 1385–1389.
59. Huang,J., Yang,X., He,X., Wang,K., Liu,J., Shi,H., Wang,Q., Guo,Q. and He,D. (2014) Design and bioanalytical applications of DNA hairpin-based fluorescent probes. *TrAC Trends Anal. Chem.*, **53**, 11–20.
60. Zhang,S., Sun,H., Chen,H., Li,Q., Guan,A., Wang,L., Shi,Y., Xu,S., Liu,M. and Tang,Y. (2018) Direct visualization of nucleolar G-quadruplexes in live cells by using a fluorescent light-up probe. *Biochim. Biophys. Acta (BBA) - Gen. Subj.*, **1862**, 1101–1106.
61. GONZÁLEZ-DOMÍNGUEZ,I., Cervera,L., Gòdia,F. and Roldán,M. (2019) Quantitative colocalization analysis of DNA delivery by PEI-mediated cationic polymers in mammalian cells. *J. Microsc.*, **273**, 53–64.
62. Dumitrache,A., Tolbert,A., Natzke,J., Brown,S.D., Davison,B.H. and Ragauskas,A.J. (2017) Cellulose and lignin colocalization at the plant cell wall surface limits microbial hydrolysis of Populus biomass. *Green Chem.*, **19**, 2275–2285.
63. Yang,M., Chen,X., Zhu,L., Lin,S., Li,C., Li,X., Huang,K. and Xu,W. (2021) Aptamer-functionalized DNA–Silver nanocluster nanofilm for visual detection and elimination of bacteria. *ACS Appl. Mater. Interfaces*, **13**, 38647–38655.